Science Advances
AAAS

Supplementary Materials for

Arresting the bad seed: HDAC3 regulates proliferation of different microglia after ischemic stroke

Yue Zhang *et al.*

Corresponding author: Yanqin Gao, yqgao@shmu.edu.cn; Ye Gong, gong_ye@fudan.edu.cn

Sci. Adv. **10**, eade6900 (2024)
DOI: 10.1126/sciadv.ade6900

The PDF file includes:

Other Supplementary Material for this manuscript includes the following:

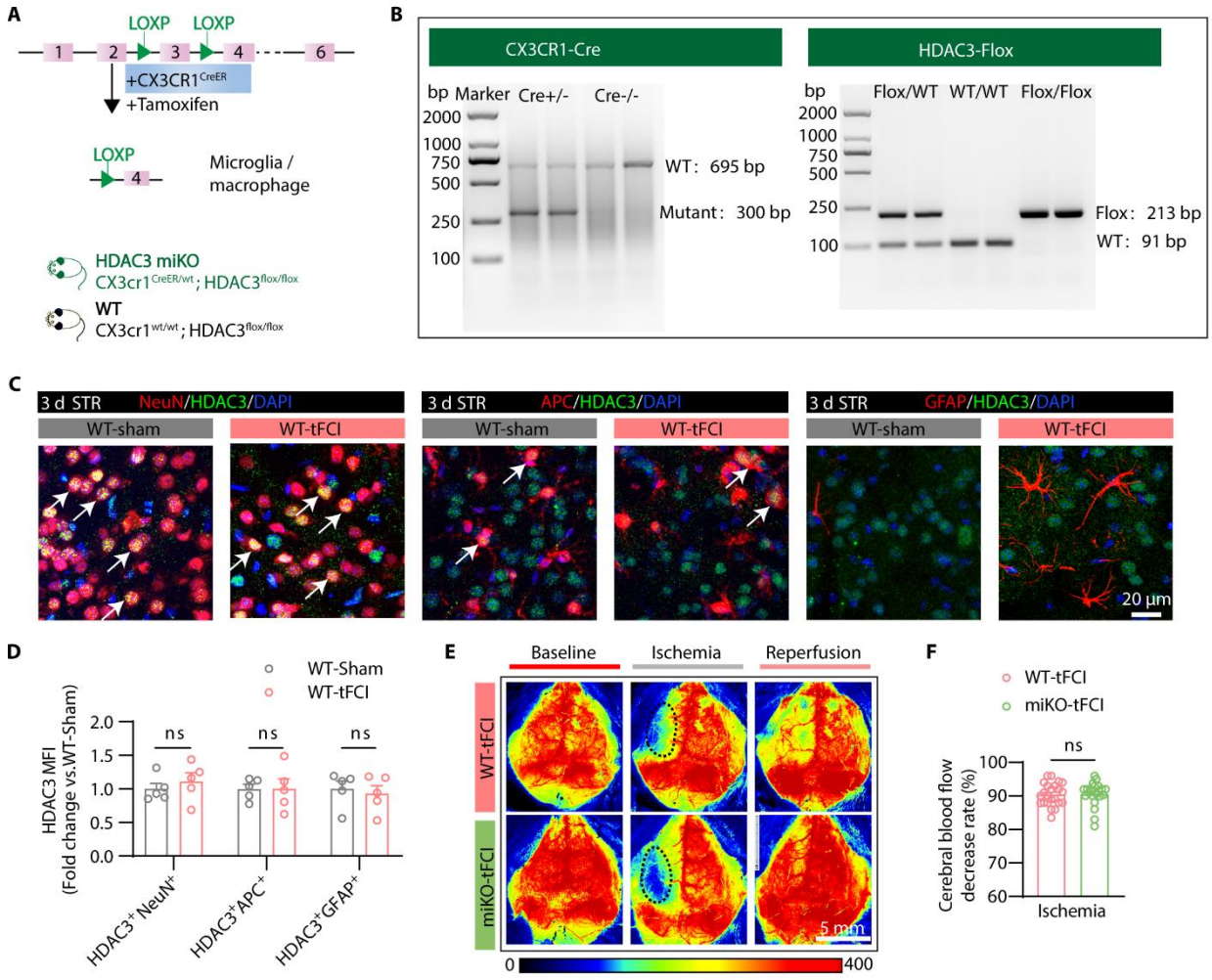

fig. S1. Construction of HDAC3-miKO transgenic mice and ischemic stroke model.

(A) Generation of tamoxifen-induced, microglia/macrophage-specific HDAC3 knockout (HDAC3-miKO) mice by crossing the CX3CR1^{CreER} mice with HDAC3$^{flox/flox}$ mice. **(B)** PCR genotyping of CX3CR1-Cre and HDAC3-Flox. **(C)** Representative immunofluorescence images taken from the peri-infarct region of striatum (STR) 3 days after tFCI showing HDAC3 colocalized with NeuN, APC, and GFAP signals, respectively. **(D)** Quantification of HDAC3 expression in neuron, oligodendrocytes, and astrocytes. n = 5-6 per group. **(E)** tFCI was induced by MCAO for 60 min in HDAC3-miKO mice and WT control mice. Laser speckle images monitored cortical cerebral blood flow (rCBF) before surgery (Baseline), 10 min after ischemia (Ischemia), and 10 min after reperfusion (Reperfusion). **(F)** rCBF was monitored with laser Doppler. n = 20-23 per group. All data are presented as the mean ± SEM. Data were analyzed using unpaired two-tailed Student's t-test (**D**) or Mann Whitney test (**F**), ns: no significance, as indicated.

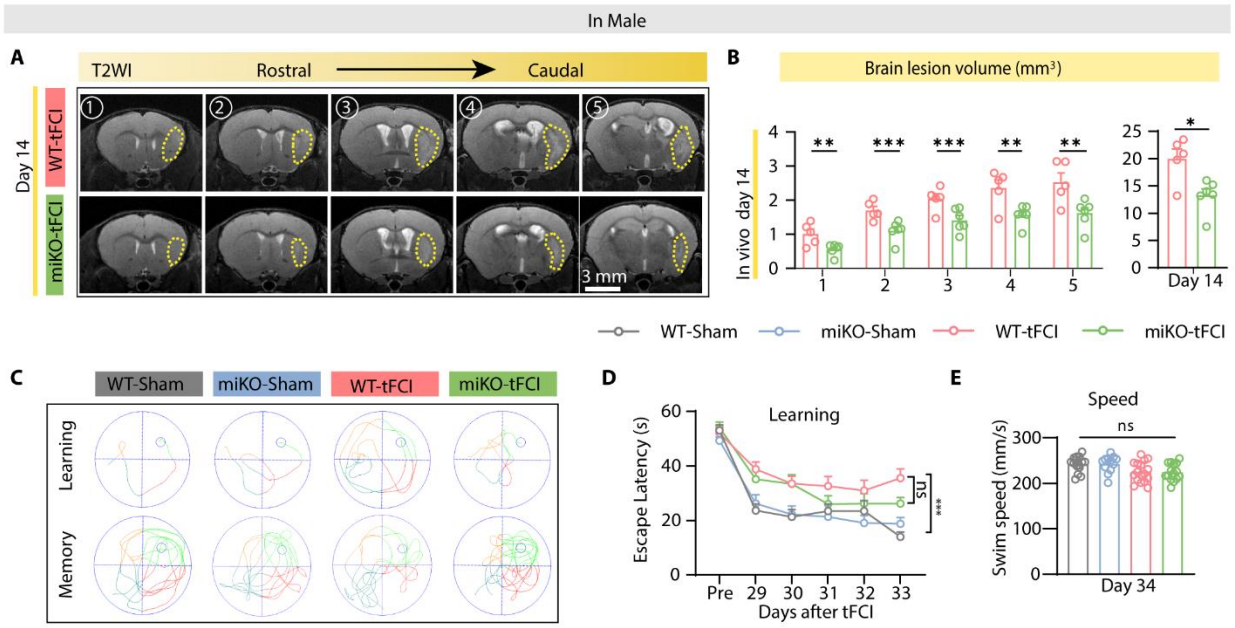

fig. S2. HDAC3-miKO attenuates histological damage and long-term behavioral deficits after stroke in males.

(A) Representative axial views (from rostral to caudal) of T2-weighted images (T2WI) 14 d after stroke. **(B)** Quantification of brain lesion volume at five axial levels from rostral to caudal (left panel) and total brain lesion volume (right panel). n = 5-6 per group. **(C)** Representative swimming paths during the learning and memory phases of the Morris water maze test. **(D)** Spatial learning was assessed by the escape latency (Pre, 29-33 d after tFCI). **(E)** All mice had similar swim speeds (34d after tFCI), reflecting comparable locomotor functions. n = 13-17 per group. All data are presented as the mean±SEM. Data were analyzed using one-way ANOVA followed by Bonferroni's post hoc tests **(E)**, GEE followed by Tukey's post hoc for repeated measures **(B left panel, D)** or unpaired two-tailed Student's t-test (**B, right panel**). *$p < 0.05$, **$p < 0.01$, ***$p < 0.001$. ns: no significance, as indicated.

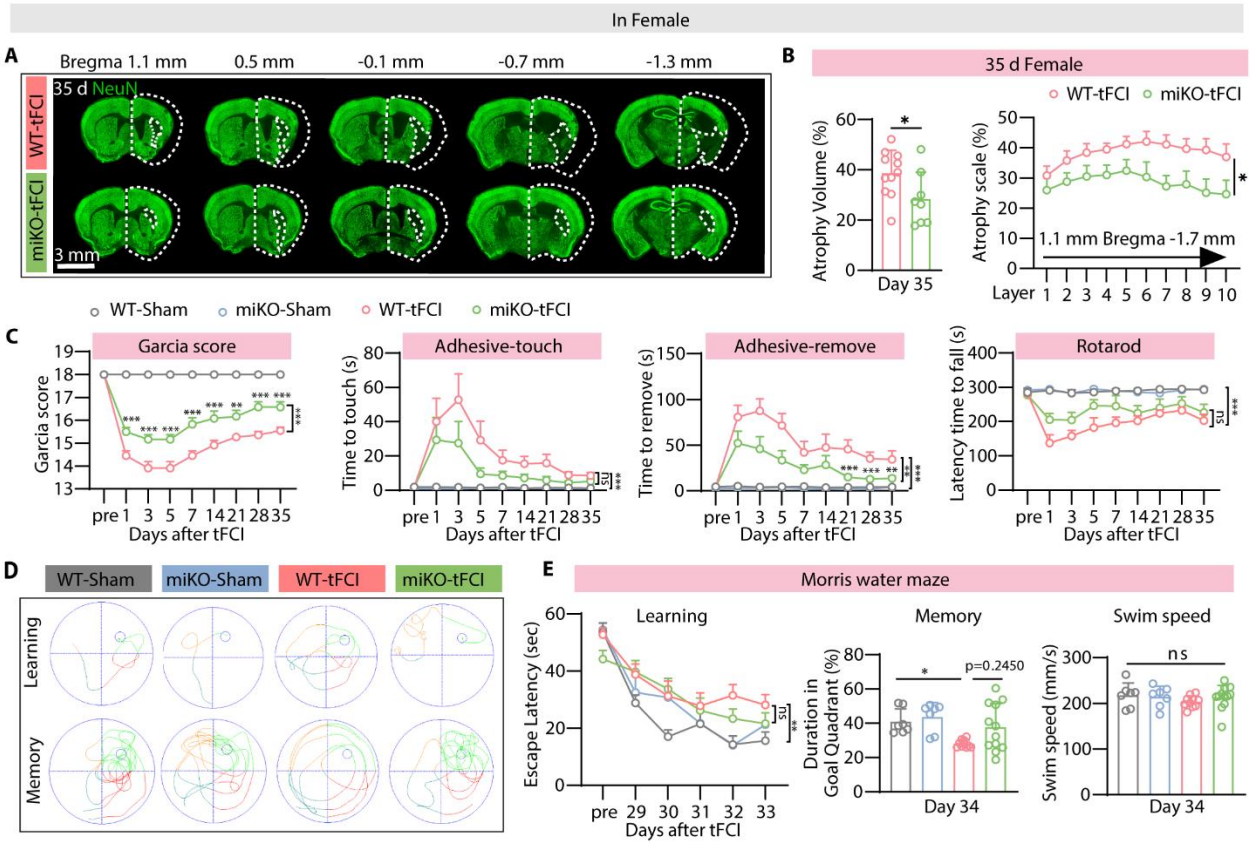

fig. S3. HDAC3-miKO attenuates histological damage and long-term behavioral deficits after stroke in females.

(A) Representative images of NeuN staining for sections. **(B)** Quantification of the atrophy volume and the area from bregma 1.1 mm-1.7 mm. n = 11 for WT-tFCI, n = 8 for miKO-tFCI. **(C)** Sensorimotor deficits were evaluated before (Pre) and up to 35 d after tFCI or Sham by the Garcia score, adhesive touch, adhesive removal test and rotarod test. n = 5-7 for WT-Sham and miKO-Sham, n = 9-12 for WT-tFCI and miKO-tFCI. **(D)** Representative swimming paths during the learning or memory phases of the Morris water maze test**. (E)** Spatial learning was assessed by the escape latency (pre, 29-33 d after tFCI) (left panel) and the memory was measured by the time spent in the target quadrant (34 d after tFCI) after removal of the platform (middle panel). All mice had similar swim speeds (34 d after tFCI), reflecting comparable locomotor functions (right panel). n = 7 for WT-/miKO-Sham, n = 10-12 for tFCI. All data are presented as the mean ± SEM. Data were analyzed using one-way ANOVA followed by Bonferroni's post hoc tests **(E right panels)**, GEE followed by Tukey's post hoc **(B** right panel**, C,** and **E** left panel**)**, Kruskal-Wallis test followed by

Dunn's multiple comparisons test **(E** right two panels**)** or unpaired two-tailed Student's t-test (**B** left panel). *$p < 0.05$, **$p < 0.01$, ***$p < 0.001$, ns: no significance, as indicated.

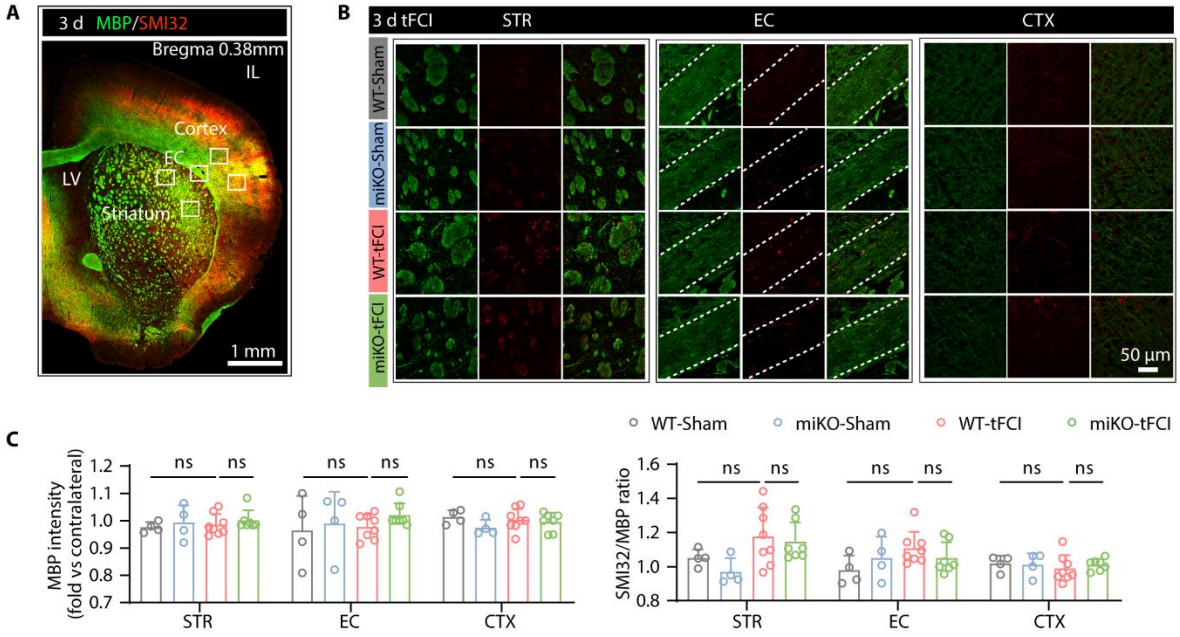

fig. S4. HDAC3-miKO has no effect on white matter injury at the acute stage of stroke.

(A) Representative image of MBP/SMI32 immunostaining in the ipsilateral hemisphere 3 d after tFCI. Boxes indicates where images in **(B)** were taken from. **(B)** Group-wise representative images of MBP/SMI32 immunostaining in the peri-infarct region of STR, EC and CTX. **(C)** The fluorescence intensity of MBP and the ratio of SMI32 to MBP immunofluorescence intensity in the STR, EC, and CTX on day 3 after tFCI. Data are normalized to the intensities of contralateral hemispheres. n = 4 for WT-Sham and miKO-Sham, n = 8 for WT-tFCI, n = 7 for miKO-tFCI. All data are presented as the mean ± SEM. Data were analyzed using one-way ANOVA followed by Bonferroni's post hoc tests or Kruskal-Wallis test followed by Dunn's multiple comparisons test. ns: no significance, as indicated.

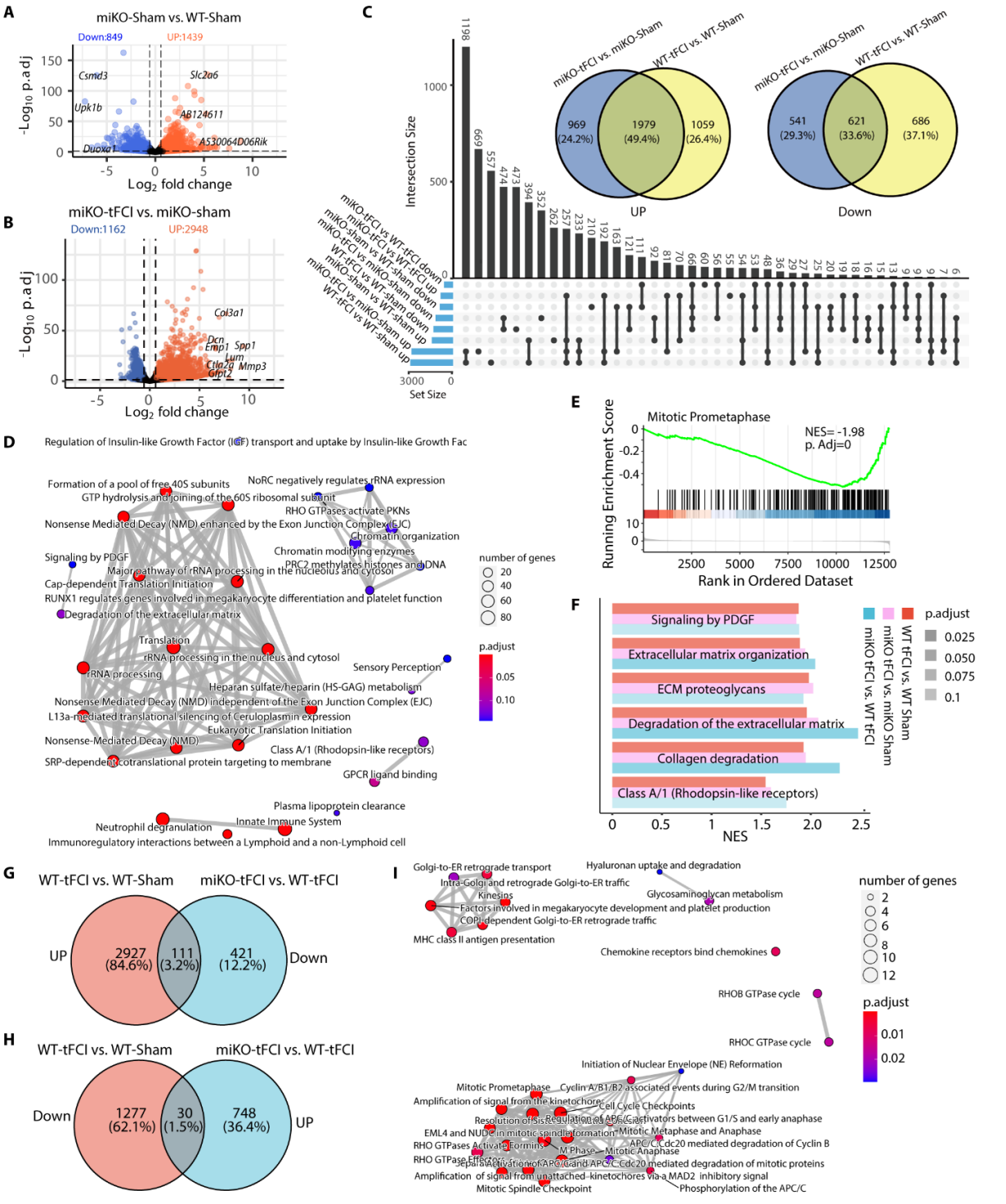

fig. S5. Effects of HDAC3-miKO on microglial gene expression under physiological conditions and in response to ischemic stroke.

(A) Volcano plot depicting DEGs in miKO-Sham *vs.* WT-Sham and **(B)** in miKO-tFCI *vs.* miKO-Sham (log2fold change > 0.58 or < -0.58, adjusted p value <0.05). **(C)** Upset diagram visualizing

overlap among all gene sets (upregulated and downregulated genes in WT-Sham, miKO-Sham, WT-tFCI and miKO-tFCI, respectively). The set size represented the total number of significant genes per gene set. The intersection size showed the number of overlapping genes in each of the respective gene set combinations, as shown by the filled dots underneath. Two venn diagrams highlighted overlaps of up-/down-regulated genes generated by miKO-tFCI *vs.* miKO-Sham and WT-tFCI *vs.* WT-Sham. **(D)** Enrichment map visualizing enriched Reactome Pathways obtained from GSEA (miKO-Sham *vs.* WT-Sham). Mutually overlapping terms clustered together. **(E)** GSEA showed significantly downregulated Reactome pathways for "Mitotic Prometaphase" (miKO-tFCI *vs.* WT-tFCI). **(F)** The remaining 6 terms from the overlap of the venn plot related to Fig. 4G. **(G-H)** Venn diagrams showed the overlap **(G)** between upregulated genes in WT-tFCI *vs.* WT-Sham (3,038 in total) and downregulated genes in miKO-tFCI *vs.* WT-tFCI (532 in total), and the overlap **(H)** between downregulated genes in WT-tFCI *vs.* WT-Sham (1,307 in total) and upregulated genes in miKO-tFCI *vs.* WT-tFCI (778 in total). **(I)** Enrichment map visualizing enriched Reactome Pathways obtained from GSEA of 111 overlapping DEGs in **(G)**. Notably, the overlapping genes in **(H)** were not enriched for any Reactome terms.

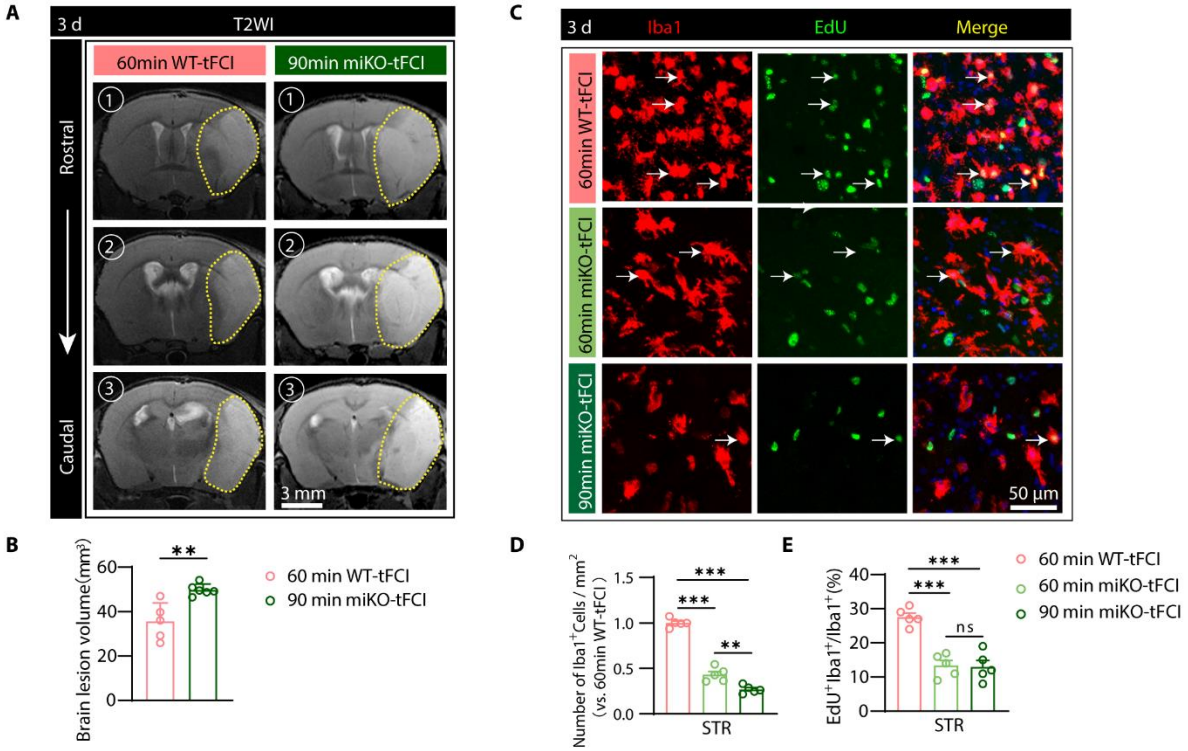

fig. S6. Evaluation of brain lesion volume and microglial proliferation following 90 min tFCI in HDAC3-miKO mice.

(A) Representative axial views (3 sections from rostral to caudal) of T2-weighted images (T2WI) at day 3 after stroke and the corresponding **(B)** Quantification of the total lesion volume. n = 5-6 per group. **(C)** Representative images of Iba1/EdU double immunostaining. White arrows indicate $Iba1^+EdU^+$ cells. **(D-E)** Quantification of $Iba1^+$ number and the proportion of EdU^+Iba1^+ cells. n = 5-6 per group. All data are presented as the mean ± SEM. Data were analyzed using unpaired with two-tailed Student's t-test **(B)** or one-way ANOVA followed by Bonferroni's post hoc tests **(D-E)**. $^{**}p < 0.01$, $^{***}p < 0.001$, ns: no significance, as indicated.

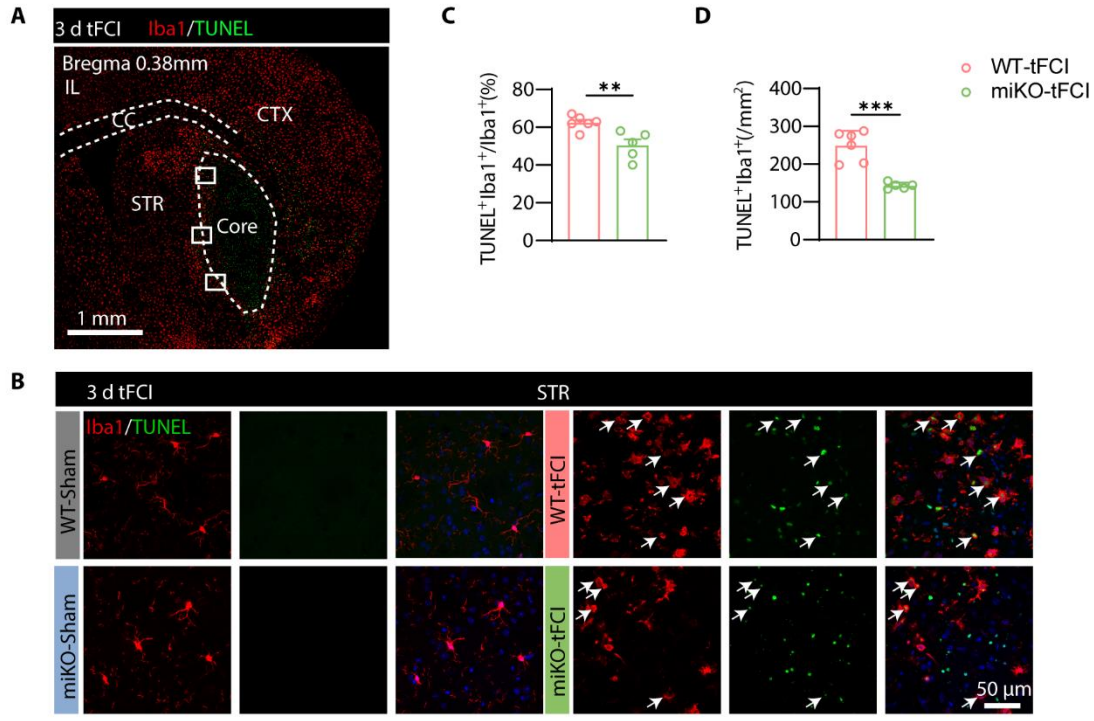

fig. S7. HDAC3-miKO inhibits microglial proliferation and apoptosis after tFCI.

(A-B) Representative images showing Iba1 immunosignal co-labeled with TUNEL (white arrows). Boxes indicate where the group-wise images were taken in the peri-infarct region of STR 3 d after tFCI **(B)**. **(C-D)** Quantification of the percentage of $Iba1^+Tunel^+$ out of the total $Iba1^+$ cells **(C)** and the numbers of $Iba1^+TUNEL^+$ cells **(D)** in the peri-infarct region of STR 3 d after tFCI. n = 5-6 per

group. All data are presented as the mean ± SEM. Data were analyzed using unpaired two-tailed Student's t-test. $^{**}p < 0.01$, $^{***}p < 0.001$, as indicated.

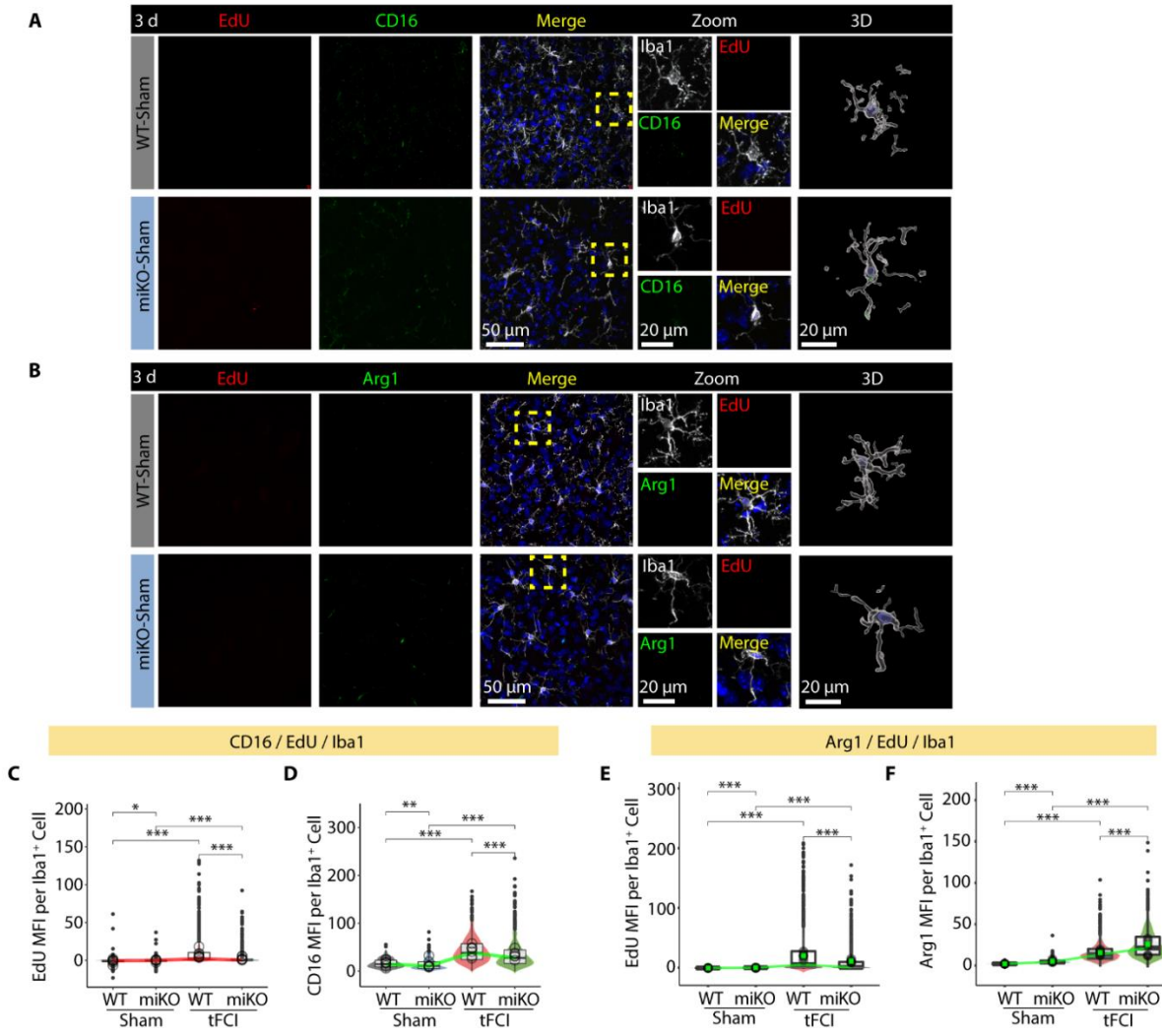

fig. S8. HDAC3-miKO inhibits the proliferation of pro-inflammatory microglia after tFCI.

(A-B) Representative images of Iba1/EdU/CD16 immunofluorescence **(A)** and Iba1/ EdU/ Arg1 **(B)** in the STR of the Sham groups. Microglia indicated by the yellow boxes were performed 3D reconstruction. EdU and CD16 signals were not detected in $Iba1^+$ cells in both Sham groups. **(C-D)** Quantification of MFI of EdU **(C)** and CD16 **(D)** per microglia. **(E-F)** Quantification of the MFI of EdU **(E)** and Arg1 **(F)** per microglia. Each black filled dot in **(C-F)** represented an individual $Iba1^+$ cell, and each hollow circle represented an individual animal. n = 5-6 per group. All data are presented as the mean ± SEM. Data were analyzed using unpaired two-tailed Student's t-test **(C-F)** $^{*}p < 0.05$, $^{**}p < 0.01$, $^{***}p < 0.001$, ns: no significance, as indicated.

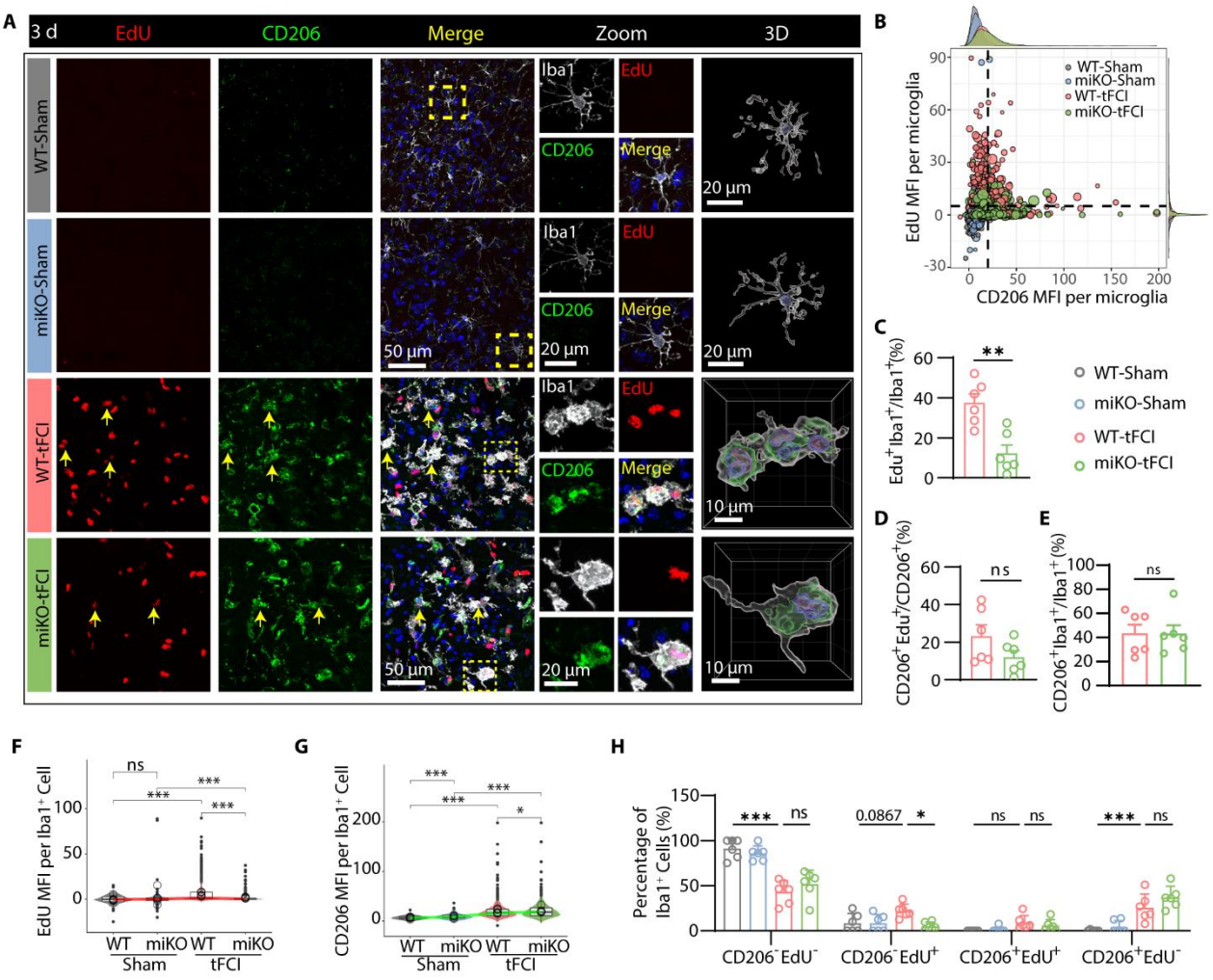

fig. S9. HDAC-miKO did not inhibit proliferation of CD206$^+$Iba1$^+$ cells after tFCI.

(A) Representative images of Iba1/EdU/CD206 immunofluorescence in the peri-infarct region of STR or in the contralateral STR 3 d after tFCI. **(B)** Scatter plot showing MFI of EdU and CD206 per microglia. **(C-D)** Quantification of the percentage of proliferating microglia (Edu$^+$Iba1$^+$, **C**) and CD206$^+$ microglia (CD206$^+$EdU$^+$/CD206$^+$, **D**). **(E)** Quantification of the percentage CD206$^+$ microglia. **(F-G)** Quantification of the MFI of EdU **(E)** and CD206 **(F)** per microglia. Each black filled dot represented an individual Iba1$^+$ cell, and each hollow circle represented an individual animal. **(H)** Quantification of the percentage of microglia with CD206$^-$EdU$^-$Iba1$^+$, CD206$^-$EdU$^+$Iba1$^+$, CD206$^+$EdU$^-$Iba1$^+$, CD206$^+$EdU$^+$Iba1$^+$. n = 6 per group. All data are presented as the mean ± SEM. Data were analyzed using unpaired with two-tailed Student's t-test **(C-G)**, or two-way ANOVA followed by Bonferroni's post hoc tests **(H)**. $^{**}p< 0.01$, $^{***}p< 0.001$, as indicated.

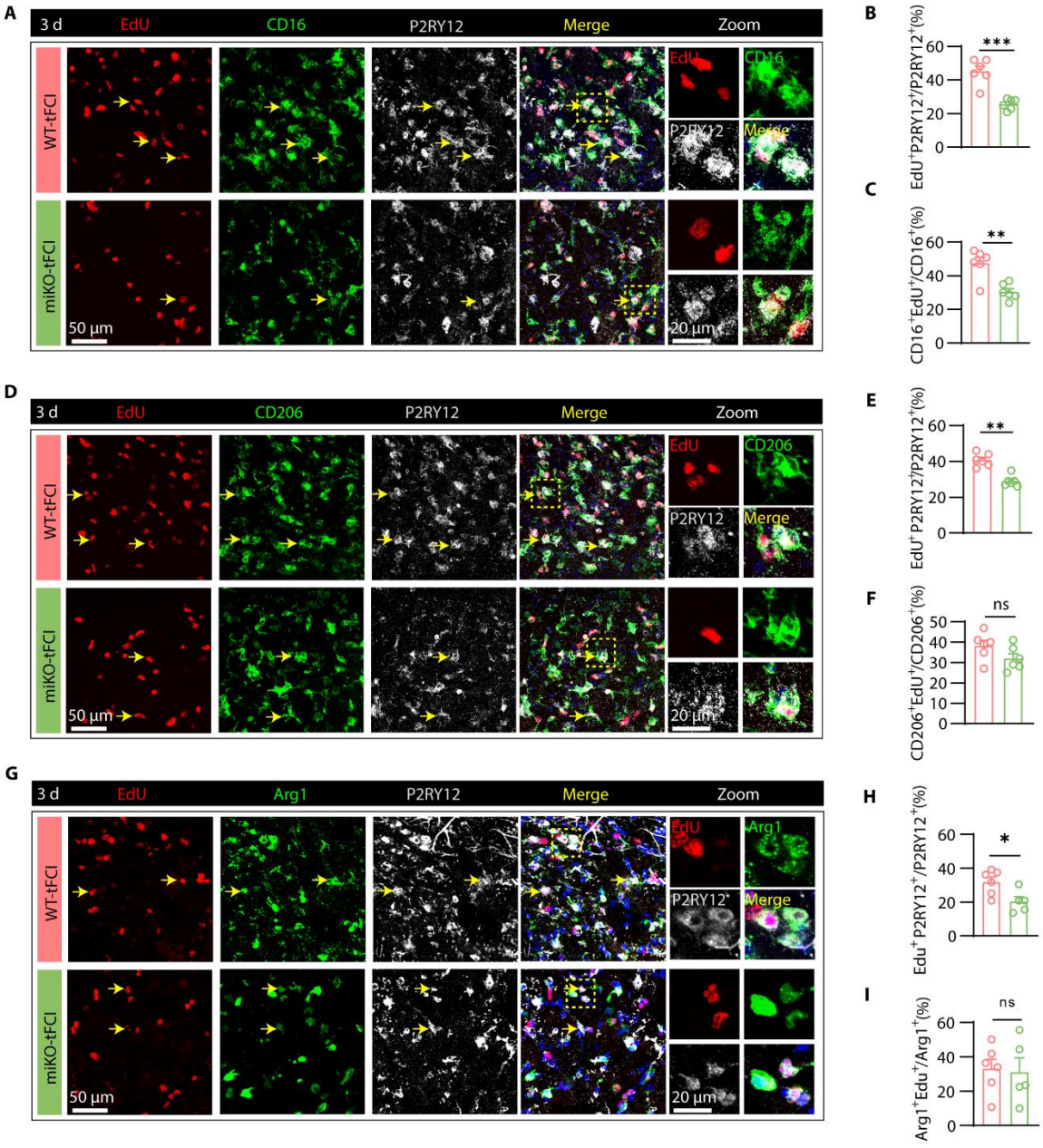

fig. S10. HDAC-miKO selectively inhibited proliferation of CD16$^+$P2RY12$^+$ cells after tFCI.

(A) Representative images of P2RY12/EdU/CD16 immunofluorescence in the peri-infarct region of STR 3 d after tFCI. **(B)** Quantification of the percentage of proliferating microglia (EdU$^+$P2RY12$^+$), in P2RY12/EdU/CD16 staining. **(C)** Quantification of the percentage of proliferating CD16$^+$P2RY12$^+$ microglia out of total CD16$^+$ cells. **(D)** Quantification of the percentage of proliferating microglia (EdU$^+$P2RY12$^+$), corresponding to P2RY12/EdU/CD206 staining. **(E)** Representative images of P2RY12/EdU/CD206 immunofluorescence in the peri-

infarct region of STR 3 days after tFCI. **(F)** Quantification of the percentage of proliferating microglia $CD206^+P2RY12^+$ microglia out of total $CD206^+$ cells. n = 6 per group. **(G)** Quantification of the percentage of proliferating microglia ($EdU^+P2RY12^+$), corresponding to P2RY12/EdU/Arg1 staining. **(H)** Representative images of P2RY12/EdU/Arg1 immunofluorescence in the peri-infarct region of STR 3 days after tFCI. **(I)** Quantification of the percentage of proliferating microglia $Arg1^+P2RY12^+$ microglia out of total $CD206^+$ cells. n = 6 per group. All data are presented as the mean ± SEM. Data were analyzed using unpaired with two-tailed Student's t-test (**B**, **C**, **F, H, I**) or Mann Whitney test (**E**). *p< 0.05, **p< 0.01, ***p< 0.001, as indicated.

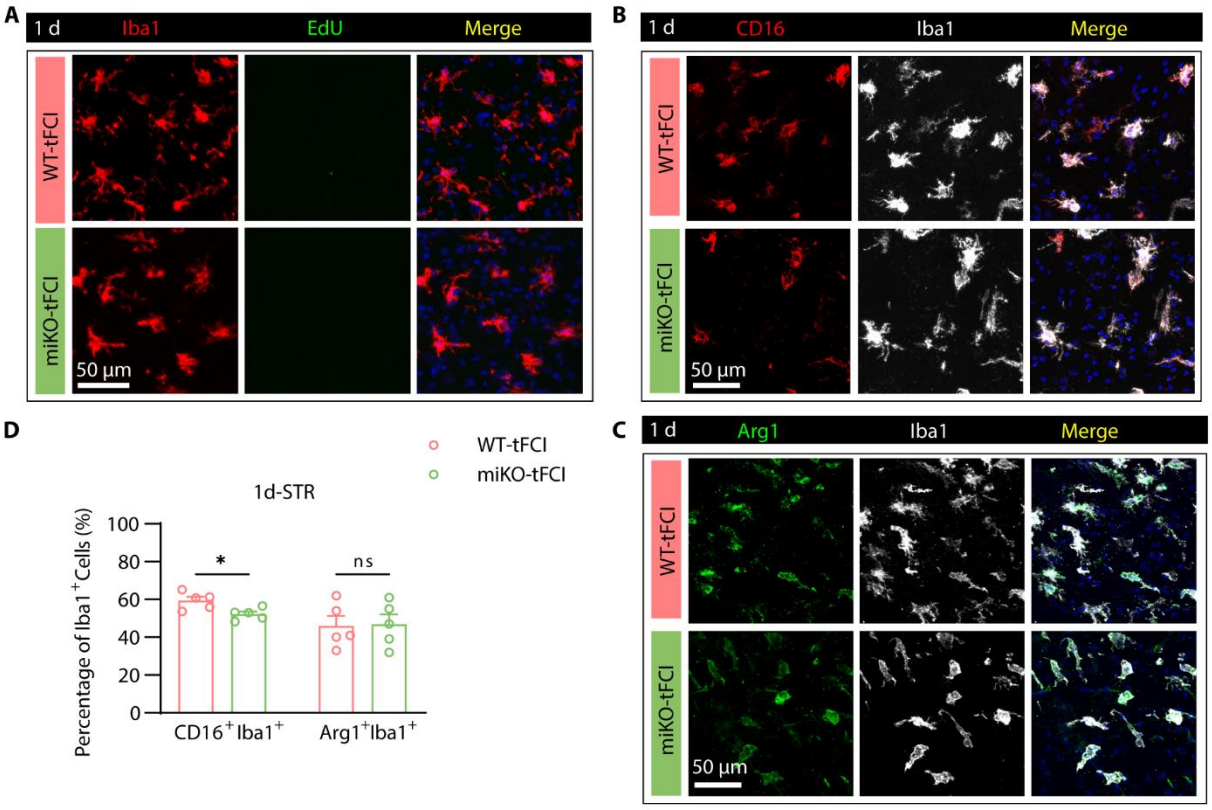

fig. S11. HDAC3-miKO inhibited microglial pro-inflammatory response as early as one day after tFCI, before significant microglial self-renewal.

(A) Representative images of Iba1/EdU immunostaining in the peri-infarct region of STR at day 1 after tFCI. Of note, EdU^+Iba1^+ signals were rarely observed so that the corresponding quantification was not shown. **(B)** Representative images of Iba1/CD16 immunostaining in the peri-infarct region of STR at day 1 after tFCI. **(C)** Representative images of Iba1/Arg1 immunostaining in the peri-infarct region of STR at day 1 after tFCI. **(D)** Quantification of $CD16^+$, $Arg1^+$ in STR 1 day after

tFCI. n = 5/group. All data are presented as the mean ± SEM. Data were analyzed using unpaired two-tailed Student's t-test. *p<0.05, ns: no significance, as indicated.

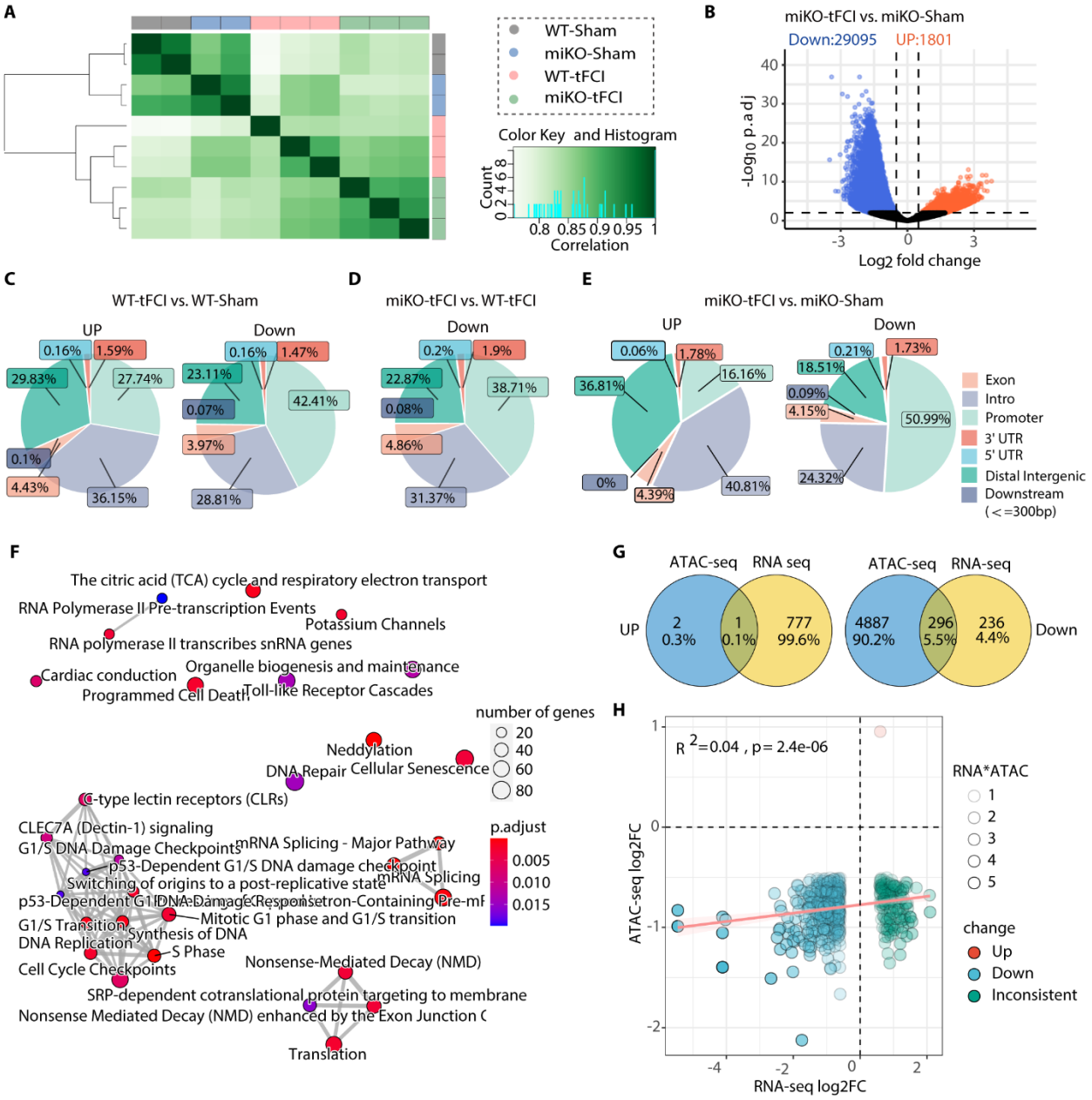

fig. S12. Integrative analysis of ATAC-seq and RNA-seq, related to Figure 7.

(A) ATAC-seq peaks correlation heatmap of all replicates. **(B)** Volcano plots showing microglia-specific differential accessibility regions (DARs; log2fold change > 0.5 or < -0.5, FDR < 0.01) in miKO-tFCI *vs.* miKO-Sham. **(C)** Pie chart showing genomic distribution of ATAC-seq peaks that

were significantly up-/down-regulated in WT-tFCI *vs.* WT-Sham. **(D)** Pie chart showing genomic distribution of ATAC-seq peaks that were significantly downregulated in miKO-tFCI *vs.* WT-tFCI. Of note, only 13 upregulated signals were detected so that the distribution of these signals was not shown. **(E)** Pie chart showing genomic distribution of ATAC-seq peaks that were significantly up-/down-regulated in miKO-tFCI *vs.* miKO-Sham. **(F)** Enrichment map visualizing enriched pathways obtained from GSEA of DARs at promoters (< 3 Kb to TSS) generated from miKO-tFCI *vs.* WT-tFCI. **(G)** Overlap between upregulated genes in RNA-seq and open DARs annotated to promoters in ATAC-seq (left panel). Overlap between downregulated genes in RNA-seq and closed DARs annotated to promoters in ATAC-seq (right panel) in miKO-tFCI *vs.* WT-tFCI. **(H)** Scatter plot showing the correlation of log2fold change of DEGs ($|\log_2\text{fold change}| > 0.58$ & adjusted *p* value < 0.05) from RNA-seq and log2fold change of their corresponding promoter-located DARs ($|\log_2\text{fold change} > 0.5$ & adjusted *p* value < 0.01) from ATAC-seq in miKO-tFCI *vs.* WT-tFCI. The transparency of each dot represents the product of RNA-seq $\log_2$fold change and ATAC-seq $\log_2$fold change.

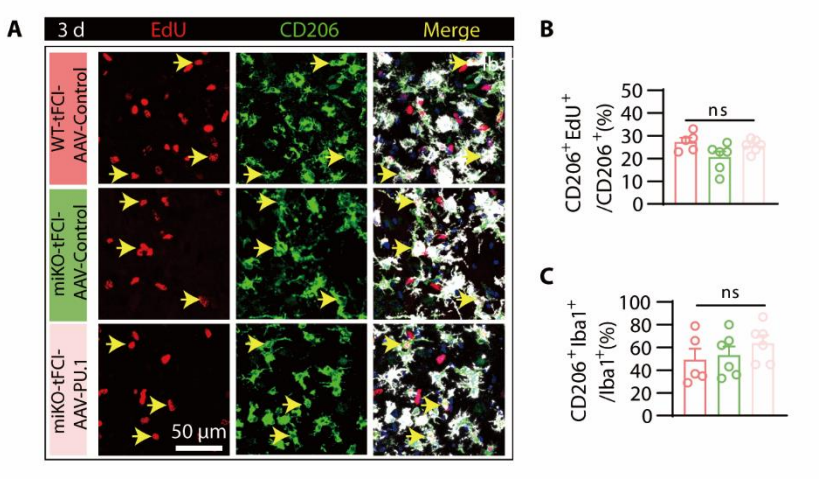

fig. S13. AAV-PU.1 did not affect CD206$^+$ microglial proliferation.

Representative images of Iba1/EdU/CD206 staining in the peri-infarct region of STR 3 days after tFCI. **(B-C)** Quantification of the percentage of different microglia, including proliferative CD206$^+$ (CD206$^+$EdU$^+$/CD206$^+$), and CD206$^+$ microglia, respectively. n=5-6 per group. All data are presented as the mean ± SEM. Data were analyzed using one-way ANOVA followed by Bonferroni's post hoc (**B, C**). ns: no significance, as indicated.

Supplementary Methods and Materials

Behavioral tests

Garcia score*:* We used an 18-point score adapted from the one developed for stroke by Garcia et al (*79*) as presented in Table S1.

Table S1. Garcia score.

Test(score)	3	2	1	0
Spontaneous activity	3-4 walls, 1-2 walls plus raise on hindlimbs	1-2 walls	Minimal movement	Akinesia
Side stroking	Bilateral brisk	Bilateral weak or ipsilateral strong and contralateral weak	Unilateral	No response
Limb symmetry	Forelimb and hindlimb extended	Mid flexion of forelimb	Contralateral forelimb flexed with hindlimb extended	Contralaterally flexed
Lateral turning	Bilateral turning >45°	Bilateral turning <45°	Unilateral turning	No turning
Forelimb walking	Bilateral turning >45°	Bilateral turning <45°	Unilateral turning	No turning
Forelimb walking	Brisk forward	Moves toward on	Movement	Hemiplegi

Rotarod test: The Rotarod test is used to evaluate the motor coordination ability and exercise tolerance of mice. The Rotarod test was performed with the Rotarod apparatus (Model 47650, Ugo Basile Srl, Varese, Italy). The mice were forced to run on a rotating drum with speeds starting at 5 rpm, accelerating to 40 rpm within 300 s. The latency to fall off the rotating rod was recorded. Data were expressed as the mean value from three trials. Mice were pre-trained 1d-3d before tFCI and data measured 1d before tFCI were recorded as preoperative data (pre). Repeat testing was performed 1d,3d, 5d, 7d, 14d, 21d, 28d, and 35d after tFCI.

Adhesive removal test*:* The adhesive removal test was assessed for forepaw sensitivity and motor impairments. The adhesive removal test was carried out with 3 × 4 mm tape. Adhesive tapes

were applied to the mouse ipsilateral or contralateral forepaw to evaluate the mice's sensory and motor function after tFCI. The time for the mouse to touch and remove the tape was measured up to 120 s. Data were presented as the mean value of three trials. Data measured 1d before tFCI were recorded as the preoperative data (pre). Repeat testing on the adhesive removal test was performed 1d, 3d, 5d, 7d, 14d, 21d, 28d, and 35d after tFCI.

Morris water maze: Memory impairment is often associated with ischemic stroke patients. Morris water maze (MWM) is used to evaluate the spatial learning and memory ability of mice(*70*). We performed MWM between 29-34 days after tFCI. During the learning phase, mice were trained on four trials (at four fixed locations) per day between 29d-33d after tFCI. In each trial, the time to reach the platform (within 60 seconds) was recorded. If the mice did not find the platform within 60 seconds, the experimenter would guide the mice to the platform and record the time as 60 seconds. At the end of a trial, the mouse was allowed to stay on the platform for 20 seconds to remember the spatial location of the platform. The memory test was performed 34 days after tFCI. The platform was removed, and a 60 s probe test was performed on each mouse. Swimming speed and time in the target quadrant were also recorded.

Table S2. Antibodies for immunofluorescence.

Antibody	Category	Dilution	Company
Iba1	019-19741	1:1000	Wako
Iba1	ab5076	1:1000	Abcam
CD206	AF2535	1:200	R&D Systems
CD16	553142	1:200	BD
HDAC3	ab32369	1:300	Abcam
NeuN	ab177487	1:1000	Abcam
Ki67	ab15580	1:500	Abcam
Alexa Fluor® 488 Anti-NeuN	ab190195	1:1000	Abcam
TUNEL	C1089	1:10	Beyotime
MBP	ab40390	1:1000	Abcam
SMI32	801701	1:1000	BioLegend
pH3	06-570	1:500	Millopore
Rat-anti-CC1 antibody	OB-PRT039	1:300	Oasisbiofarm
GFAP	PA5-18598	1:1000	Thermo
PU.1	2258	1:500	CST
P2RY12	69766	1:500	CST
mCherry	M11217	1:1000	Thermo
Arg1	SC-271430	1:50	Santa Cruz
Alexa Fluor® 488 AffiniPure Donkey Anti-Rabbit IgG (H+L)	711-545-152	1:1000	Jackson
Alexa Fluor® 488 AffiniPure Goat Anti-Rat IgG (H+L)	112-545-003	1:1000	Jackson
Alexa Fluor® 488 AffiniPure Donkey Anti-Goat IgG (H+L)	705-545-147	1:1000	Jackson
Cy™3 AffiniPure Donkey Anti-Rabbit IgG (H+L)	711-165-152	1:1000	Jackson
Cy™3 AffiniPure Donkey Anti-Rat IgG (H+L)	712-165-153	1:1000	Jackson
Cy™3 AffiniPure Goat Anti-Mouse IgG (H+L)	115-165-146	1:1000	Jackson
Alexa Fluor® 647 AffiniPure Donkey Anti-Rabbit IgG (H+L)	711-605-152	1:1000	Jackson
Alexa Fluor® 647 AffiniPure Donkey Anti-Rat IgG (H+L)	712-605-153	1:1000	Jackson
Alexa Fluor® 647 AffiniPure Donkey Anti-Goat IgG (H+L)	705-605-147	1:1000	Jackson

Table S3. Primer sequences for qRT-PCR.

Gene	Primer sequences
Gapdh	Forward: GTGAAGGTCGGTGTGAACGG; Reverse: GTTTCCCGTTGATGACCAG
Tnf-α	Forward: GACCCTCACACTCAGATCATCTTCT; Reverse: CCTCCACTTGGTGGTTTGCT
Cxcl-10	Forward: CCAAGTGCTGCCGTCATTTTC; Reverse: GGCTCGCAGGGATGATTTCAA
Il-1β	Forward: CTCCATGAGCTTTGTACAAGG; Reverse: TGCTGATGTACCAGTTGGGG
Il-1α	Forward: CGAAGACTACAGTTCTGCCATT; Reverse: GACGTTTCAGAGGTTCTCAGAG
NFKbib	Forward: GCGGATGCCGATGAATGGT; Reverse: TGACGTAGCCAAAGACTAAGGG
Kntc1	Forward: TATTGAGCTGCTAACAAGCGATG; Reverse: ACTGACTGGTCTGCAACGATTA
Ccl-22	Forward: CTGATGCAGGTCCCTATGGT; Reverse: GCAGGATTTTGAGGTCCAGA
Arg1	Forward: TCACCTGAGCTTTGATGTCG; Reverse: CTGAAAGGAGCCCTGTCTTG
Ccl7	Forward: GCTGCTTTCAGCATCCAAGTG; Reverse: CCAGGGACACCGACTACTG
Itgax	Forward: CTGGATAGCCTTTCTTCTGCTG; Reverse: GCACACTGTGTCCGAACTCA
Mmp12	Forward: CATGAAGCGTGAGGATGTAGAC; Reverse: TGGGCTAGTGTACCACCTTTG
Cdca8	Forward: AAAAGCGAAAGGTAATCGAGGT; Reverse: TGCAGATCGAAGATTCTTATGGC
Ki67	Forward: ATCATTGACCGCTCCTTTAGGT; Reverse: GCTCGCCTTGATGGTTCCT
Birc5	Forward: GAGGCTGGCTTCATCCACTG; Reverse: ATGCTCCTCTATCGGGTTGTC
PU.1	Forward: TACTGGGATTTCTCCGCACAC; Reverse: GTGGCGATAGAGCTGCTGTAG
Pcna	Forward: TTGCACGTATATGCCGAGACC; Reverse: GGTGAACAGGCTCATTCATCTCT
Cdk2	Forward: CTCTCACGGGCATTCCTCTTC; Reverse: CCCTCTGCATTGATAAGCAGG
CyclinE1	Forward: GAAAAGCGAGGATAGCAGTCAG;

	Reverse: CCCAATTCAAGACGGGAAGTG
Cdk1	Forward: AGAAGGTACTTACGGTGTGGT; Reverse: GAGAGATTTCCCGAATTGCAGT
Sgo1	Forward: TCTATCCGTCGCCATTTAAGGA; Reverse: GCAGGGTTACGGTTACTTCTC

Table S4. Antibodies for flow cytometry.

Antibody	Category	Dilution	Company
DyeCycle dye	R37172	1：100	Thermo
anti-CD45-eFluor450	48-0451-82	1：100	Thermo
anti-CD11b-(APC)-cy7	47-0112-82	1：100	Thermo
anti-F4/80-BUV395	565614	1：100	BD
anti-O4-APC	130-119-155	1：100	Miltenyi
anti-β-tubulin-Percp-cy5.5	801215	1：100	BioLegend
CD11c-PerCP cy5.5	45-0114-82	1：100	Thermo
Ly6G(Gr1)-PE	12-9669-82	1：100	Thermo

Appendix Data S1: Data of Statistical information.

Appendix Data S2: The Top 100 downregulated genes in Fig. 4H.

REFERENCES AND NOTES

1. N. Gu, J. Peng, M. Murugan, X. Wang, U. B. Eyo, D. Sun, Y. Ren, E. DiCicco-Bloom, W. Young, H. Dong, L.-J. Wu, Spinal microgliosis due to resident microglial proliferation is required for pain hypersensitivity after peripheral nerve injury. *Cell Rep.* **16**, 605–614 (2016).

2. A. Olmos-Alonso, S. T. T. Schetters, S. Sri, K. Askew, R. Mancuso, M. Vargas-Caballero, C. Holscher, V. H. Perry, D. Gomez-Nicola, Pharmacological targeting of CSF1R inhibits microglial proliferation and prevents the progression of Alzheimer's-like pathology. *Brain* **139**, 891–907 (2016).

3. J. Jia, L. Yang, Y. Chen, L. Zheng, Y. Chen, Y. Xu, M. Zhang, The role of microglial phagocytosis in ischemic stroke. *Front. Immunol.* **12**, 790201 (2021).

4. M. W. Sieber, N. Jaenisch, M. Brehm, M. Guenther, B. Linnartz-Gerlach, H. Neumann, O. W. Witte, C. Frahm, Attenuated inflammatory response in triggering receptor expressed on myeloid cells 2 (TREM2) knock-out mice following stroke. *PLOS ONE* **8**, e52982 (2013).

5. C. Barca, C. Foray, S. Hermann, U. Herrlinger, I. Remory, D. Laoui, M. Schäfers, O. M. Grauer, B. Zinnhardt, A. H. Jacobs, The colony stimulating factor-1 receptor (CSF-1R)-mediated regulation of microglia/macrophages as a target for neurological disorders (glioma, stroke). *Front. Immunol.* **12**, 787307 (2021).

6. T. Li, J. Zhao, W. Xie, W. Yuan, J. Guo, S. Pang, W.-B. Gan, D. Gómez-Nicola, S. Zhang, Specific depletion of resident microglia in the early stage of stroke reduces cerebral ischemic damage. *J. Neuroinflammation* **18**, 81 (2021).

7. S. Wahane, X. Zhou, X. Zhou, L. Guo, M.-S. Friedl, M. Kluge, A. Ramakrishnan, L. Shen, C. C. Friedel, B. Zhang, R. H. Friedel, H. Zou, Diversified transcriptional responses of myeloid and glial cells in spinal cord injury shaped by HDAC3 activity. *Sci. Adv.* **7**, eabd8811 (2021).

8. M. J. Emmett, M. A. Lazar, Integrative regulation of physiology by histone deacetylase 3. *Nat. Rev. Mol. Cell Biol.* **20**, 102–115 (2019).

9. Y. Liao, J. Cheng, X. Kong, S. Li, X. Li, M. Zhang, H. Zhang, T. Yang, Y. Dong, J. Li, Y. Xu, Z. Yuan, HDAC3 inhibition ameliorates ischemia/reperfusion-induced brain injury by regulating the microglial cGAS-STING pathway. *Theranostics* **10**, 9644–9662 (2020).

10. Y. Zhao, H. Mu, Y. Huang, S. Li, Y. Wang, R. A. Stetler, M. V. L. Bennett, C. E. Dixon, J. Chen, Y. Shi, Microglia-specific deletion of histone deacetylase 3 promotes inflammation resolution, white matter integrity, and functional recovery in a mouse model of traumatic brain injury. *J. Neuroinflammation* **19**, 201 (2022).

11. G. Wang, Y. Shi, X. Jiang, R. K. Leak, X. Hu, Y. Wu, H. Pu, W.-W. Li, B. Tang, Y. Wang, Y. Gao, P. Zheng, M. V. L. Bennett, J. Chen, HDAC inhibition prevents white matter injury by modulating microglia/macrophage polarization through the GSK3β/PTEN/Akt axis. *Proc. Natl. Acad. Sci. U.S.A.* **112**, 2853–2858 (2015).

12. N. Adhikari, T. Jha, B. Ghosh, Dissecting histone deacetylase 3 in multiple disease conditions: Selective inhibition as a promising therapeutic strategy. *J. Med. Chem.* **64**, 8827–8869 (2021).

13. K. Kierdorf, D. Erny, T. Goldmann, V. Sander, C. Schulz, E. G. Perdiguero, P. Wieghofer, A. Heinrich, P. Riemke, C. Hölscher, D. N. Müller, B. Luckow, T. Brocker, K. Debowski, G. Fritz, G. Opdenakker, A. Diefenbach, K. Biber, M. Heikenwalder, F. Geissmann, F. Rosenbauer, M. Prinz, Microglia emerge from erythromyeloid precursors via Pu.1- and Irf8-dependent pathways. *Nat. Neurosci.* **16**, 273–280 (2013).

14. P. B. Staber, P. Zhang, M. Ye, R. S. Welner, C. Nombela-Arrieta, C. Bach, M. Kerenyi, B. A. Bartholdy, H. Zhang, M. Alberich-Jordà, S. Lee, H. Yang, F. Ng, J. Zhang, M. Leddin, L. E. Silberstein, G. Hoefler, S. H. Orkin, B. Göttgens, F. Rosenbauer, G. Huang, D. G. Tenen, Sustained PU.1 levels balance cell-cycle regulators to prevent exhaustion of adult hematopoietic stem cells. *Mol. Cell* **49**, 934–946 (2013).

15. A. A. Pimenova, M. Herbinet, I. Gupta, S. I. Machlovi, K. R. Bowles, E. Marcora, A. M. Goate, Alzheimer's-associated PU.1 expression levels regulate microglial inflammatory response. *Neurobiol. Dis.* **148**, 105217 (2021).

16. E. D. Ponomarev, T. Veremeyko, N. Barteneva, A. M. Krichevsky, H. L. Weiner, MicroRNA-124 promotes microglia quiescence and suppresses EAE by deactivating macrophages via the C/EBP-α-PU.1 pathway. *Nat. Med.* **17**, 64–70 (2011).

17. R. Lin, Y. Zhou, T. Yan, R. Wang, H. Li, Z. Wu, X. Zhang, X. Zhou, F. Zhao, L. Zhang, Y. Li, M. Luo, Directed evolution of adeno-associated virus for efficient gene delivery to microglia. *Nat. Methods* **19**, 976–985 (2022).

18. S. Baltan, A. Bachleda, R. S. Morrison, S. P. Murphy, Expression of histone deacetylases in cellular compartments of the mouse brain and the effects of ischemia. *Transl. Stroke Res.* **2**, 411–423 (2011).

19. E. Shosha, R. A. Shahror, C. A. Morris, Z. Xu, R. Lucas, M. E. McGee-Lawrence, N. J. Rusch, R. B. Caldwell, A. Y. Fouda, The arginase 1/ornithine decarboxylase pathway suppresses HDAC3 to ameliorate the myeloid cell inflammatory response: Implications for retinal ischemic injury. *Cell Death Dis.* **14**, 621 (2023).

20. M. S. Mendes, L. Le, J. Atlas, Z. Brehm, A. Ladron-de-Guevara, E. Matei, C. Lamantia, M. N. McCall, A. K. Majewska, The role of P2Y12 in the kinetics of microglial self-renewal and maturation in the adult visual cortex in vivo. *eLife* **10**, e61173 (2021).

21. T. Li, S. Pang, Y. Yu, X. Wu, J. Guo, S. Zhang, Proliferation of parenchymal microglia is the main source of microgliosis after ischaemic stroke. *Brain* **136**, 3578–3588 (2013).

22. D. Birenbaum, L. W. Bancroft, G. J. Felsberg, Imaging in acute stroke. *West. J. Emerg. Med.* **12**, 67–76 (2011).

23. F. Sohrabji, A. Okoreeh, A. Panta, Sex hormones and stroke: Beyond estrogens. *Horm. Behav.* **111**, 87–95 (2019).

24. A. Villa, P. Gelosa, L. Castiglioni, M. Cimino, N. Rizzi, G. Pepe, F. Lolli, E. Marcello, L. Sironi, E. Vegeto, A. Maggi, Sex-specific features of microglia from adult mice. *Cell Rep.* **23**, 3501–3511 (2018).

25. D. Chen, J. Li, Y. Huang, P. Wei, W. Miao, Y. Yang, Y. Gao, Interleukin 13 promotes long-term recovery after ischemic stroke by inhibiting the activation of STAT3. *J. Neuroinflammation* **19**, 112 (2022).

26. X. Hu, P. Li, Y. Guo, H. Wang, R. K. Leak, S. Chen, Y. Gao, J. Chen, Microglia/macrophage polarization dynamics reveal novel mechanism of injury expansion after focal cerebral ischemia. *Stroke* **43**, 3063–3070 (2012).

27. H. C. B. Nguyen, M. Adlanmerini, A. K. Hauck, M. A. Lazar, Dichotomous engagement of HDAC3 activity governs inflammatory responses. *Nature* **584**, 286–290 (2020).

28. M. Boyce, Y. Xin, O. Chowdhury, P. Shang, H. Liu, V. Koontz, A. Strizhakova, M. Nemani, S. Hose, J. S. Zigler, M. Campbell, D. Sinha, J. T. Handa, K. Kaarniranta, J. Qian, S. Ghosh, Microglia–neutrophil interactions drive dry AMD-like pathology in a mouse model. *Cell* **11**, 3535 (2022).

29. Y. Takeda, P. He, I. Tachibana, B. Zhou, K. Miyado, H. Kaneko, M. Suzuki, S. Minami, T. Iwasaki, S. Goya, T. Kijima, T. Kumagai, M. Yoshida, T. Osaki, T. Komori, E. Mekada, I. Kawase, Double deficiency of tetraspanins CD9 and CD81 alters cell motility and protease production of macrophages and causes chronic obstructive pulmonary disease-like phenotype in mice. *J. Biol. Chem.* **283**, 26089–26097 (2008).

30. Y. Jiang, J. Hsieh, HDAC3 controls gap 2/mitosis progression in adult neural stem/progenitor cells by regulating CDK1 levels. *Proc. Natl. Acad. Sci. U.S.A.* **111**, 13541–13546 (2014).

31. M. Vidal-Laliena, E. Gallastegui, F. Mateo, M. Martínez-Balbás, M. J. Pujol, O. Bachs, Histone deacetylase 3 regulates cyclin A stability. *J. Biol. Chem.* **288**, 21096–21104 (2013).

32. R. Matheson, K. Chida, H. Lu, V. Clendaniel, M. Fisher, A. Thomas, E. H. Lo, M. Selim, A. Shehadah, Neuroprotective effects of selective inhibition of histone deacetylase 3 in experimental stroke. *Transl. Stroke Res.* **11**, 1052–1063 (2020).

33. J.-Y. Kim, H. S. Jeong, T. Chung, M. Kim, J. H. Lee, W. H. Jung, J. S. Koo, The value of phosphohistone H3 as a proliferation marker for evaluating invasive breast cancers: A comparative study with Ki67. *Oncotarget* **8**, 65064–65076 (2017).

34. M. J. Hoffmann, S. Meneceur, K. Hommel, W. A. Schulz, G. Niegisch, Downregulation of cell cycle and checkpoint genes by class I HDAC inhibitors limits synergism with G2/M checkpoint inhibitor MK-1775 in bladder cancer cells. *Genes* **12**, 260 (2021).

35. G. E. Holder, C. M. McGary, E. M. Johnson, R. Zheng, V. T. John, C. Sugimoto, M. J. Kuroda, W. K. Kim, Expression of the mannose receptor CD206 in HIV and SIV encephalitis: A phenotypic switch of brain perivascular macrophages with virus infection. *J. Neuroimmune Pharmacol.* **9**, 716–726 (2014).

36. G. Faraco, L. Park, J. Anrather, C. Iadecola, Brain perivascular macrophages: Characterization and functional roles in health and disease. *J. Mol. Med.* **95**, 1143–1152 (2017).

37. K. Bartalska, V. Hübschmann, M. Korkut-Demirbaş, R. J. A. Cubero, A. Venturino, K. Rössler, T. Czech, S. Siegert, A systematic characterization of microglia-like cell occurrence during retinal organoid differentiation. *iScience* **25**, 104580 (2022).

38. M. R. Corces, A. Shcherbina, S. Kundu, M. J. Gloudemans, L. Frésard, J. M. Granja, B. H. Louie, T. Eulalio, S. Shams, S. T. Bagdatli, M. R. Mumbach, B. Liu, K. S. Montine, W. J. Greenleaf, A. Kundaje, S. B. Montgomery, H. Y. Chang, T. J. Montine, Single-cell epigenomic analyses implicate candidate causal variants at inherited risk loci for Alzheimer's and Parkinson's diseases. *Nat. Genet.* **52**, 1158–1168 (2020).

39. R. R. Starks, A. Biswas, A. Jain, G. Tuteja, Combined analysis of dissimilar promoter accessibility and gene expression profiles identifies tissue-specific genes and actively repressed networks. *Epigenetics Chromatin* **12**, 16 (2019).

40. A. M. Smith, H. M. Gibbons, R. L. Oldfield, P. M. Bergin, E. W. Mee, R. L. M. Faull, M. Dragunow, The transcription factor PU.1 is critical for viability and function of human brain microglia. *Glia* **61**, 929–942 (2013).

41. S. E. Mullican, C. A. Gaddis, T. Alenghat, M. G. Nair, P. R. Giacomin, L. J. Everett, D. Feng, D. J. Steger, J. Schug, D. Artis, M. A. Lazar, Histone deacetylase 3 is an epigenomic brake in macrophage alternative activation. *Genes Dev.* **25**, 2480–2488 (2011).

42. A. Sanyal, B. R. Lajoie, G. Jain, J. Dekker, The long-range interaction landscape of gene promoters. *Nature* **489**, 109–113 (2012).

43. J. Rustenhoven, A. M. Smith, L. C. Smyth, D. Jansson, E. L. Scotter, M. E. V. Swanson, M. Aalderink, N. Coppieters, P. Narayan, R. Handley, C. Overall, T. I. H. Park, P. Schweder, P. Heppner, M. A. Curtis, R. L. M. Faull, M. Dragunow, PU.1 regulates Alzheimer's disease-associated genes in primary human microglia. *Mol. Neurodegener.* **13**, 44 (2018).

44. R. Sarkar, S. Banerjee, S. A. Amin, N. Adhikari, T. Jha, Histone deacetylase 3 (HDAC3) inhibitors as anticancer agents: A review. *Eur. J. Med. Chem.* **192**, 112171 (2020).

45. A. R. Summers, M. A. Fischer, K. R. Stengel, Y. Zhao, J. F. Kaiser, C. E. Wells, A. Hunt, S. Bhaskara, J. W. Luzwick, S. Sampathi, X. Chen, M. A. Thompson, D. Cortez, S. W. Hiebert, HDAC3 is essential for DNA replication in hematopoietic progenitor cells. *J. Clin. Invest.* **123**, 3112–3123 (2013).

46. A. K. Singh, A. Bishayee, A. K. Pandey, Targeting histone deacetylases with natural and synthetic agents: An emerging anticancer strategy. *Nutrients* **10**, 731 (2018).

47. W. Tan, P.-Y. P. Su, J. Leff, X. Gao, J. Chen, A. K. Guan, G. Kalyanasundaram, A. Ma, Z. Guan, Distinct phases of adult microglia proliferation: A Myc-mediated early phase and a Tnfaip3-mediated late phase. *Cell Discov.* **8**, 34 (2022).

48. F. C. Grandi, H. Modi, L. Kampman, M. R. Corces, Chromatin accessibility profiling by ATAC-seq. *Nat. Protoc.* **17**, 1518–1552 (2022).

49. R. N. Laribee, M. J. Klemsz, Loss of PU.1 expression following inhibition of histone deacetylases. *J. Immunol.* **167**, 5160–5166 (2001).

50. Y. Koyama, M. Adachi, M. Sekiya, M. Takekawa, K. Imai, Histone deacetylase inhibitors suppress IL-2-mediated gene expression prior to induction of apoptosis. *Blood* **96**, 1490–1495 (2000).

51. W. Jian, B. Yan, S. Huang, Y. Qiu, Histone deacetylase 1 activates PU.1 gene transcription through regulating TAF9 deacetylation and transcription factor IID assembly. *FASEB J.* **31**, 4104–4116 (2017).

52. R. N. Laribee, M. J. Klemsz, Histone H4 HDAC activity is necessary for expression of the PU.1 gene. *Biochim. Biophys. Acta* **1730**, 226–234 (2005).

53. G. Huang, P. Zhang, H. Hirai, S. Elf, X. Yan, Z. Chen, S. Koschmieder, Y. Okuno, T. Dayaram, J. D. Growney, R. A. Shivdasani, D. G. Gilliland, N. A. Speck, S. D. Nimer, D. G. Tenen, PU.1 is a major downstream target of AML1 (RUNX1) in adult mouse hematopoiesis. *Nat. Genet.* **40**, 51–60 (2008).

54. A. Celada, F. E. Borràs, C. Soler, J. Lloberas, M. Klemsz, C. van Beveren, S. McKercher, R. A. Maki, The transcription factor PU.1 is involved in macrophage proliferation. *J. Exp. Med.* **184**, 61–69 (1996).

55. G. Li, W. Hao, W. Hu, Transcription factor PU.1 and immune cell differentiation (Review). *Int. J. Mol. Med.* **46**, 1943–1950 (2020).

56. S.-F. Lau, C. Chen, W.-Y. Fu, J. Y. Qu, T. H. Cheung, A. K. Y. Fu, N. Y. Ip, IL-33-PU.1 transcriptome reprogramming drives functional state transition and clearance activity of microglia in Alzheimer's disease. *Cell Rep.* **31**, 107530 (2020).

57. N. Zhou, K. Liu, Y. Sun, Y. Cao, J. Yang, Transcriptional mechanism of IRF8 and PU.1 governs microglial activation in neurodegenerative condition *Cell* **10**, 87–103 (2019).

58. X. Chen, I. Barozzi, A. Termanini, E. Prosperini, A. Recchiuti, J. Dalli, F. Mietton, G. Matteoli, S. Hiebert, G. Natoli, Requirement for the histone deacetylase Hdac3 for the inflammatory gene expression program in macrophages. *Proc. Natl. Acad. Sci. U.S.A.* **109**, E2865–E2874 (2012).

59. K. Askew, K. Li, A. Olmos-Alonso, F. Garcia-Moreno, Y. Liang, P. Richardson, T. Tipton, M. A. Chapman, K. Riecken, S. Beccari, A. Sierra, Z. Molnár, M. S. Cragg, O. Garaschuk, V. H. Perry, D. Gomez-Nicola, Coupled proliferation and apoptosis maintain the rapid turnover of microglia in the adult brain. *Cell Rep.* **18**, 391–405 (2017).

60. M. C. Kodali, H. Chen, F.-F. Liao, Temporal unsnarling of brain's acute neuroinflammatory transcriptional profiles reveals panendothelitis as the earliest event preceding microgliosis. *Mol. Psychiatry* **26**, 3905–3919 (2021).

61. G. Szalay, B. Martinecz, N. Lénárt, Z. Környei, B. Orsolits, L. Judák, E. Császár, R. Fekete, B. L. West, G. Katona, B. Rózsa, Á. Dénes, Microglia protect against brain injury and their selective elimination dysregulates neuronal network activity after stroke. *Nat. Commun.* **7**, 11499 (2016).

62. A. Otxoa-de-Amezaga, F. Miró-Mur, J. Pedragosa, M. Gallizioli, C. Justicia, N. Gaja-Capdevila, F. Ruíz-Jaen, A. Salas-Perdomo, A. Bosch, M. Calvo, L. Márquez-Kisinousky, A. Denes, M. Gunzer, A. M. Planas, Microglial cell loss after ischemic stroke favors brain neutrophil accumulation. *Acta Neuropathol.* **137**, 321–341 (2019).

63. E. F. Willis, K. P. A. MacDonald, Q. H. Nguyen, A. L. Garrido, E. R. Gillespie, S. B. R. Harley, P. F. Bartlett, W. A. Schroder, A. G. Yates, D. C. Anthony, S. Rose-John, M. J. Ruitenberg, J. Vukovic, Repopulating microglia promote brain repair in an IL-6-dependent manner. *Cell* **180**, 833–846.e16 (2020).

64. W.-N. Jin, S. X.-Y. Shi, Z. Li, M. Li, K. Wood, R. J. Gonzales, Q. Liu, Depletion of microglia exacerbates postischemic inflammation and brain injury. *J. Cereb. Blood Flow Metab.* **37**, 2224–2236 (2017).

65. M. R. P. Elmore, A. R. Najafi, M. A. Koike, N. N. Dagher, E. E. Spangenberg, R. A. Rice, M. Kitazawa, B. Matusow, H. Nguyen, B. L. West, K. N. Green, Colony-stimulating factor 1 receptor signaling is necessary for microglia viability, unmasking a microglia progenitor cell in the adult brain. *Neuron* **82**, 380–397 (2014).

66. D. Gómez-Nicola, N. L. Fransen, S. Suzzi, V. H. Perry, Regulation of microglial proliferation during chronic neurodegeneration. *J. Neurosci.* **33**, 2481–2493 (2013).

67. T. R. Hammond, C. Dufort, L. Dissing-Olesen, S. Giera, A. Young, A. Wysoker, A. J. Walker, F. Gergits, M. Segel, J. Nemesh, S. E. Marsh, A. Saunders, E. Macosko, F. Ginhoux, J. Chen, R. J. M. Franklin, X. Piao, S. A. McCarroll, B. Stevens, Single-cell RNA sequencing of microglia throughout the mouse lifespan and in the injured brain reveals complex cell-state changes. *Immunity* **50**, 253–271.e6 (2019).

68. C. Böttcher, S. Schlickeiser, M. A. M. Sneeboer, D. Kunkel, A. Knop, E. Paza, P. Fidzinski, L. Kraus, G. J. L. Snijders, R. S. Kahn, A. R. Schulz, H. E. Mei, E. M. Hol, B. Siegmund, R. Glauben, E. J. Spruth, L. D. de Witte, J. Priller, Human microglia regional heterogeneity and phenotypes determined by multiplexed single-cell mass cytometry. *Nat. Neurosci.* **22**, 78–90 (2019).

69. M. J. C. Jordão, R. Sankowski, S. M. Brendecke, Sagar, G. Locatelli, Y. H. Tai, T. L. Tay, E. Schramm, S. Armbruster, N. Hagemeyer, O. Groß, D. Mai, Ö. Çiçek, T. Falk, M. Kerschensteiner, D. Grün, M. Prinz, Single-cell profiling identifies myeloid cell subsets with distinct fates during neuroinflammation. *Science* **363**, eaat7554 (2019).

70. V. Stratoulias, R. Ruiz, S. Kanatani, A. M. Osman, L. Keane, J. A. Armengol, A. Rodríguez-Moreno, A. N. Murgoci, I. García-Domínguez, I. Alonso-Bellido, F. González Ibáñez, K. Picard, G. Vázquez-Cabrera, M. Posada-Pérez, N. Vernoux, D. Tejera, K. Grabert, M. Cheray, P. González-Rodríguez, E. M. Pérez-Villegas, I. Martínez-Gallego, A. Lastra-Romero, D. Brodin, J. Avila-Cariño, Y. Cao, M. Airavaara, P. Uhlén, M. T. Heneka, M. Tremblay, K. Blomgren, J. L. Venero, B. Joseph, ARG1-expressing microglia show a distinct molecular signature and modulate postnatal development and function of the mouse brain. *Nat. Neurosci.* **26**, 1008–1020 (2023).

71. J. D. Cherry, J. A. Olschowka, M. K. O'Banion, Arginase 1+ microglia reduce Aβ plaque deposition during IL-1β-dependent neuroinflammation. *J. Neuroinflammation* **12**, 203 (2015).

72. W. Cai, X. Dai, J. Chen, J. Zhao, M. Xu, L. Zhang, B. Yang, W. Zhang, M. Rocha, T. Nakao, J. Kofler, Y. Shi, R. A. Stetler, X. Hu, J. Chen, STAT6/Arg1 promotes microglia/macrophage efferocytosis and inflammation resolution in stroke mice. *JCI Insight* **4**, e131355 (2019).

73. J. S. Kim, M. Kolesnikov, S. Peled-Hajaj, I. Scheyltjens, Y. Xia, S. Trzebanski, Z. Haimon, A. Shemer, A. Lubart, H. Van Hove, L. Chappell-Maor, S. Boura-Halfon, K. Movahedi, P. Blinder, S. Jung, A binary cre transgenic approach dissects microglia and cns border-associated macrophages. *Immunity* **54**, 176–190.e7 (2021).

74. S. De Schepper, J. Z. Ge, G. Crowley, L. S. S. Ferreira, D. Garceau, C. E. Toomey, D. Sokolova, J. Rueda-Carrasco, S.-H. Shin, J.-S. Kim, T. Childs, T. Lashley, J. J. Burden, M. Sasner, C. Sala Frigerio, S. Jung, S. Hong, Perivascular cells induce microglial phagocytic states and synaptic engulfment via SPP1 in mouse models of Alzheimer's disease. *Nat. Neurosci.* **26**, 406–415 (2023).

75. C. Kilkenny, D. G. Altman, Improving bioscience research reporting: ARRIVE-ing at a solution. *Lab. Anim*. **44**, 377–378 (2010).

76. M. Stephens, False discovery rates: A new deal. *Biostatistics* **18**, 275–294 (2016).

77. G. Yu, L.-G. Wang, Y. Han, Q.-Y. He, clusterProfiler: An R package for comparing biological themes among gene clusters. *OMICS* **16**, 284–287 (2012).

78. G. Yu, L. G. Wang, Q. Y. He, ChIPseeker: An R/bioconductor package for ChIP peak annotation, comparison and visualization. *Bioinformatics* **31**, 2382–2383 (2015).

79. J. H. Garcia, S. Wagner, K. F. Liu, X. J. Hu, Neurological deficit and extent of neuronal necrosis attributable to middle cerebral artery occlusion in rats. *Stroke* **26**, 627–634 (1995).